The structure of a neutralized virus: canine parvovirus complexed with neutralizing antibody fragment

William R Wikoff[1], Guoji Wang[1†], Colin R Parrish[2], R Holland Cheng[1], M Lisa Strassheim[2], Timothy S Baker[1] and Michael G Rossmann[1*]

[1]Department of Biological Sciences, Purdue University, West Lafayette, IN 47907-1392, USA and [2]Institute for Animal Health, New York State College of Veterinary Medicine, Cornell University, Ithaca, NY 14853, USA

Background: Members of the *Parvovirus* genus cause a variety of diseases in mammals, including humans. One of the major defences against viral infection is the presence of neutralizing antibodies that prevent virus particles from infecting target cells. The mechanism of neutralization is not well understood. We therefore studied the structure of canine parvovirus (CPV) complexed with the Fab fragment of a neutralizing antibody, A3B10, using image reconstruction of electron micrographs of vitrified samples, together with the already known structure of CPV from X-ray crystallographic data.

Results: The structure of the complex of CPV with Fab A3B10 has been determined to 23 Å resolution. The known CPV atomic structure was subtracted from the electron density of the complex, and the difference map was used to fit the atomic coordinates of a known Fab fragment, HyHEL-5. The long axis of each Fab molecule is oriented in a near radial direction, inclined away from the two-fold axes. The viral epitope consists of 14 amino acid residues found in loops 1, 2 and 3 on the capsid surface, which include previously identified escape mutations.

Conclusions: The mode of Fab binding suggests that the A3B10 neutralizing antibody cannot bind bivalently to the capsid across the two-fold axes, consistent with the observation that whole A3B10 antibody readily precipitates CPV. Since Fab A3B10 can also neutralize the virus, mechanisms of neutralization such as interference with cell attachment, cell entry, or uncoating, must be operative.

Structure 15 July 1994, **2**:595–607

Key words: antibody–virus complex, antigenic surface, cryo-electron microscopy, neutralization of virus, parvovirus

Introduction

Members of the *Parvovirus* genus cause a variety of diseases in mammals, including humans, particularly in pregnant females and in newborns. Diseases include enteritis, in the case of canine parvovirus (CPV) [1,2], and childhood fifth disease, caused by the human pathogen B19 [3,4]. Parvoviruses infect only actively proliferating (S phase) cells [5]. They have a diameter of approximately 255 Å, a molecular mass between 5.0×10^6 and 6.2×10^6 daltons, contain a single-stranded DNA genome of about 5000 bases and have a $T=1$ icosahedral capsid. The structural motif of each of the 60 capsid subunits is an eight-stranded antiparallel β-barrel, common to most icosahedral viruses [6]. CPV is most closely related to feline panleukopenia virus (FPV), raccoon parvovirus and mink enteritis virus. The major capsid component is virus protein 2 (VP2), with a small amount of VP3. VP3 results from a proteolytic cleavage of approximately 17 residues from the amino terminus of VP2 [7,8]. In CPV, VP1 contains 143 additional amino-terminal residues compared with VP2. The three-dimensional structures of CPV and FPV have been determined to atomic resolution [6,9] and of human B19 to 8 Å resolution (M Agbandje, S Kajigaya, R McKenna, NS Young & MG Rossmann, unpublished data), using X-ray crystallography.

The immune system in vertebrates is the primary mechanism by which infectious viruses are detected and neutralized. Several hypotheses have been proposed to explain how neutralization occurs [10]. For example, antibodies might bind monovalently to a virus and thereby achieve interparticle cross-linking and precipitation of the infectious particles. Alternatively, some neutralizing antibodies bind bivalently. In the case of human rhinovirus 14 (HRV14), the neutralizing monoclonal antibody (Mab) Mab17-1A binds across the icosahedral two-fold axes, thus maintaining the two-fold symmetry of the antibody [10,11]. Thus, in this instance, neutralization is not accompanied by precipitation of the virus; the mechanism of neutralization might be inhibition of receptor recruitment, of uncoating, or of other factors. Antibody fragment (Fab) Fab17 1A bridges the HRV14 canyon, which is the site of receptor binding, and thus might neutralize the virus by blocking a sufficient number of receptor attachment sites [10].

Neutralizing antigenic sites have been determined on the CPV surface, using escape mutant analysis and peptide mapping [12–15] (Table 1, Fig. 1). Two epitopes (A and B) have been identified by analysis of mutations which inhibit antibody neutralization. Site A is on the three-fold spike, involving loops 1 and 2. Site B is on a ridge between the canyon and the depression

*Corresponding author. †Present address: Department of Pathology, Scaife Hall Room A-521, University of Pittsburgh School of Medicine, Pittsburgh, PA 15261, USA.

© Current Biology Ltd ISSN 0969-2126

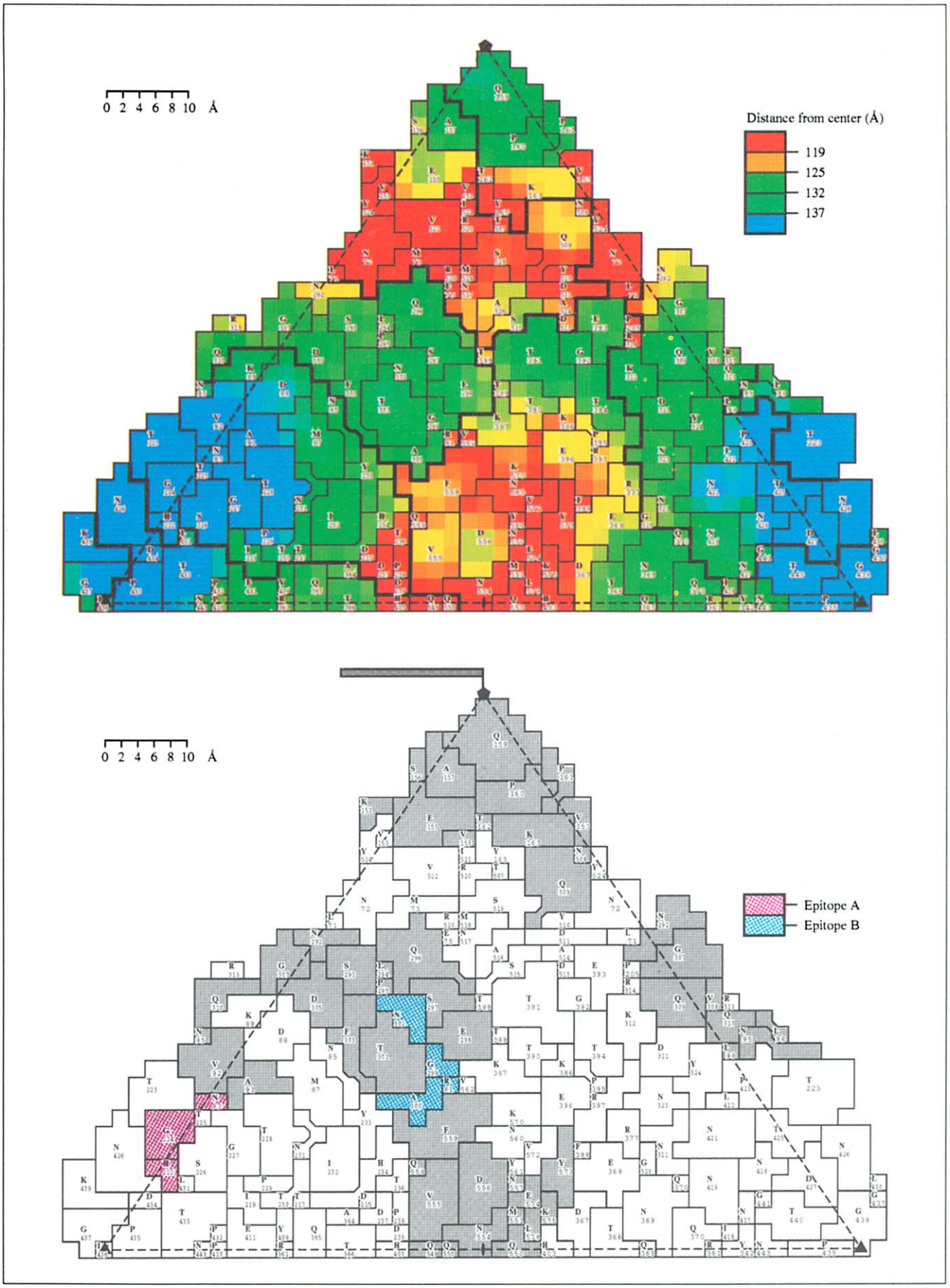
0 2 4 6 8 10 Å
Distance from center (Å)
119
125
132
137
0 2 4 6 8 10 Å
Epitope A
Epitope B

Fig. 1.(opposite). Roadmap showing the surface amino acids of CPV for one asymmetric unit of the icosahedral particle. The radial distance of the surface from the viral center is color-coded at the top. Boundaries between symmetry-related polypeptides are indicated with a heavy black line. The lower figure shows (shaded) epitopes identified by pepscan or peptide mapping. Epitopes on the amino terminus of VP1 identified by pepscan and not present in the atomic structure are indicated as a line from the five-fold axis. Escape mutations to Mab A3B10 are indicated in red (epitope A) and blue (epitope B). (The figure was produced in part by the program Roadmap [46]).

at the two-fold axis. Epitopes corresponding roughly to sites A and B have also been identified by pepscan mapping [12–14]. Additional antigenic sites have been identified by peptide mapping. Epitopes in the amino terminus of VP1, corresponding to residue positions −2 to +21 in VP2, bind antibodies that neutralize CPV. These residues may protrude through the five-fold axes [6].

Here we present the structure of a CPV:Fab complex at 23 Å resolution from which we determine the nature of the binding interface between epitope B on the virus surface and the Fab. We show that monovalent attachment is probably the mode of Mab binding.

Results and discussion

Cryo-electron microscope (EM) images were obtained of CPV complexed with ~60 Fab fragments of the neutralizing monoclonal antibody A3B10 (Fig. 2). The images were combined to produce a three-dimensional electron density map (Fig. 3). The map was then fitted with the known atomic structure of CPV and the homologous structure of Fab HyHEL-5.

Interpretation of an atomic resolution protein electron density map requires knowledge of bond lengths, bond angles, dihedral angles, planarity of chemical groups as well as amino acid sequence information. These constraints permit the placement of atomic positions with an accuracy far greater than would be possible if only the electron density map were available. For the CPV:Fab structure, atomic level information is available for the structure of CPV as well as of an Fab model with an elbow angle similar to that observed in the image reconstruction of the complex. Thus, the accuracy with which the final structure was known, after refinement of the rigid body components [10,16], permitted placement of individual amino acid groups with confidence, although the resolution of the EM reconstruction was only 23 Å (Fig. 4).

Description of the map

The 60 Fabs in the A3B10:CPV complex protrude from the virus with their long axes in a roughly radial direction (Fig. 3), and lean away from the nearest two-fold axes. The mean density of the Fab region was equal to the mean density of the CPV shell, indicating that the particles were nearly or completely saturated with Fab. The surface features of the virion in the complex are consistent with the features of the CPV capsid in the atomic structure (Fig. 5). Thus, there is no evidence for conformational changes at this resolution. The morphology of the Fab is also consistent with known Fab atomic structures (Fig. 4). The resolution of the reconstruction is sufficient to discern that the Fab is composed of four domains with a depression at the elbow between the variable and constant dimers.

The Fab footprint on the viral surface

The accurate position of the antibody footprint is dependent upon obtaining the correct hand of the struc-

Table 1. CPV epitopes.

Epitope identifier	Antigenic amino acids (VP2 numbering)	Method of identification	Ability of antibody or antiserum to neutralize CPV	Antibody type	References
A	G224, H222, N93	escape mutations	yes	monoclonal	[15,30]
B	A300, N302, G299	escape mutations	yes	monoclonal	[15,30]
1	−2 to 9	pepscan	yes	polyclonal	[13]
2	7 to 17	pepscan	yes	polyclonal	[13]
3	8 to 21	pepscan	yes	monoclonal	[13]
4	91 to 104	pepscan	yes	polyclonal	[13]
5	172 to 183	pepscan	yes	polyclonal	[13]
6	283 to 297	pepscan	Mab 4AG6 no Mab 3C10 weak	monoclonal	[13]
7	297 to 310	pepscan	yes	polyclonal	[13]
8	498 to 509	pepscan	yes	polyclonal	[13]
9	549 to 559	pepscan	yes	polyclonal	[13]
10	573 to 583	pepscan	yes	polyclonal	[13]
H-2	147 to 163	recombinant fusion protein and synthetic peptides	yes	monoclonal	[12]

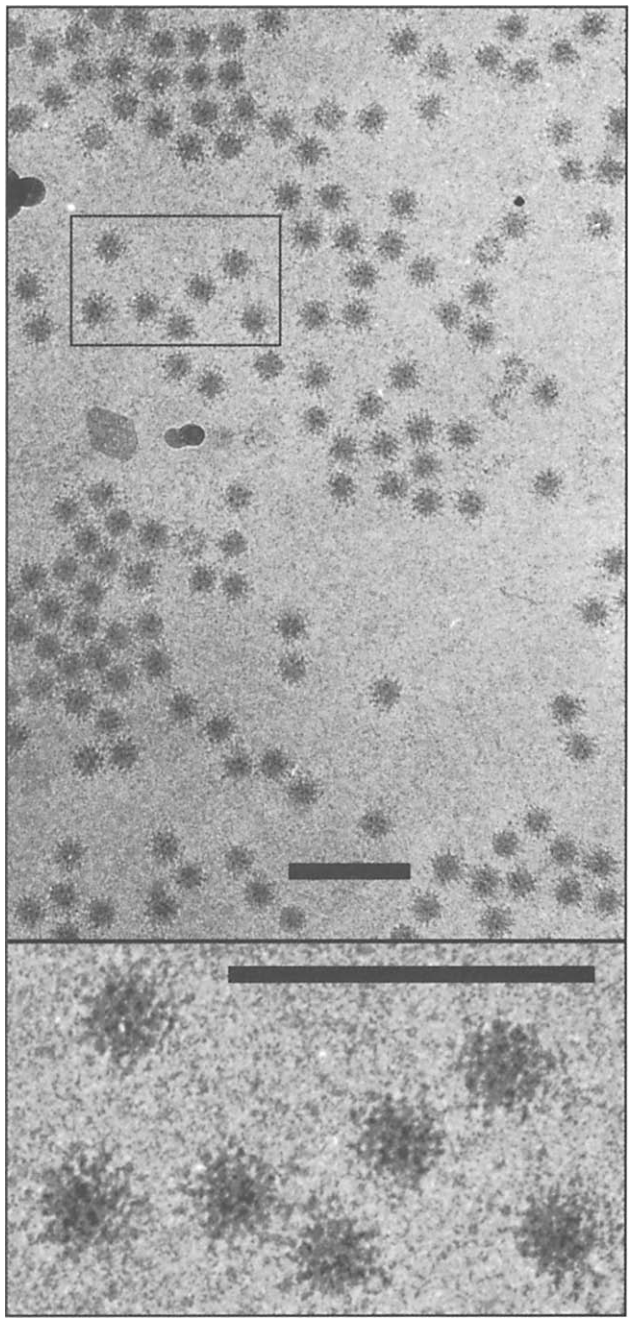

Fig. 2. Micrograph of a frozen-hydrated sample of CPV complexed with Fab A3B10. The boxed region in the top image is shown enlarged three times in the bottom image. The scale bars indicate 1000 Å.

ture and precise docking of the atomic models into the EM density map. The hand of the EM map was easily determined by visual comparison of the asymmetric features such as the curved arms of the 'pinwheel' (triskelion) feature about the three-fold axes (Fig. 3). An R-factor calculation, showing a difference of 16% between the two possibilities, verified the choice of hand.

A difference electron density map, computed by subtracting the atomic model of the CPV capsid from the EM reconstruction of the CPV:Fab complex, isolated the Fab electron density. Four lobes corresponded to the heavy- and light-chain variable and constant domains. The two lobes that form the antigen-binding surface straddle a ridge on the CPV surface composed of residues 296 to 303. Thus, even at this resolution, the complementarity between the shapes of the antibody and virus is readily apparent.

The surface area on CPV that is buried by formation of the complex is ~796 Å^2 if examined with a 1.7 Å radius probe [17]. This compares well with the lysozyme surface area that is buried when complexed with HyHEL-5 [18,19]. In general, Fab–protein contacts cover surface areas of between 690 Å^2 and 916 Å^2 using a 1.7 Å probe [20].

The footprint of the Fab molecule on CPV was determined by identifying those CPV residues which had one or more non-hydrogen atoms within specified distances of the fitted homologous HyHEL-5 Fab molecule (Table 2). For comparison, the number of lysozyme residues that contact HyHEL-5 are shown in Fig. 6, using the same distance cutoffs. The number of residues of lysozyme in contact with HyHEL-5 was also determined after a radial translation of lysozyme by 1.00 Å and 1.56 Å away from the Fab molecule. The 1.56 Å translation produces a result comparable with that in the footprint of HyHEL-5 on CPV. At the resolution of the EM map (23 Å), this translation should not be significant. Therefore, a larger distance cutoff (5 Å) than would be used in an atomic resolution structure for determining intermolecular contacts is used here for determining the antibody footprint. It is also possible that if the atomic resolution structure of A3B10, with its longer CDRs (Fig. 7), had been used in the fitting process, there would have been more contacts.

Table 2. The intermolecular contacts between CPV and the HyHEL-5 model after positional refinement.

Distance cutoff (Å)	No. of residues	Names of residues[a]
3.4	3	M87,T301,N302
3.7	5	M87,A300,T301,N302,F303
4.0	5	M87,A300,T301,N302,F303
4.5	10	N85,M87,N231,I232,Y233,S297,A300,T301,N302,F303
4.7	12	N85,M87,N231,I232,Y233,S297,A300,T301,N302,F303, T390,T391
5.0	14	N85,M87,N231,I232,Y233,Q296,S297,G299,A300,T301, N302,F303,T390,T391

[a]The CPV residues that have atomic contacts within the specified cutoff.

The escape mutations to A3B10 that have been identified cluster within the footprint of the Fab, as shown in the roadmaps (Figs 1 and 8). Residues in the footprint of Fab A3B10 on CPV include the known escape mutations (Gly299→Glu, Ala300→Val, Ala300→Asp and Asn302→Asp) to Mab A3B10, which are all on loop 3 of VP2. While mutation of residue Ala300 to valine inhibits neutralization by Mab A3B10, the mutation

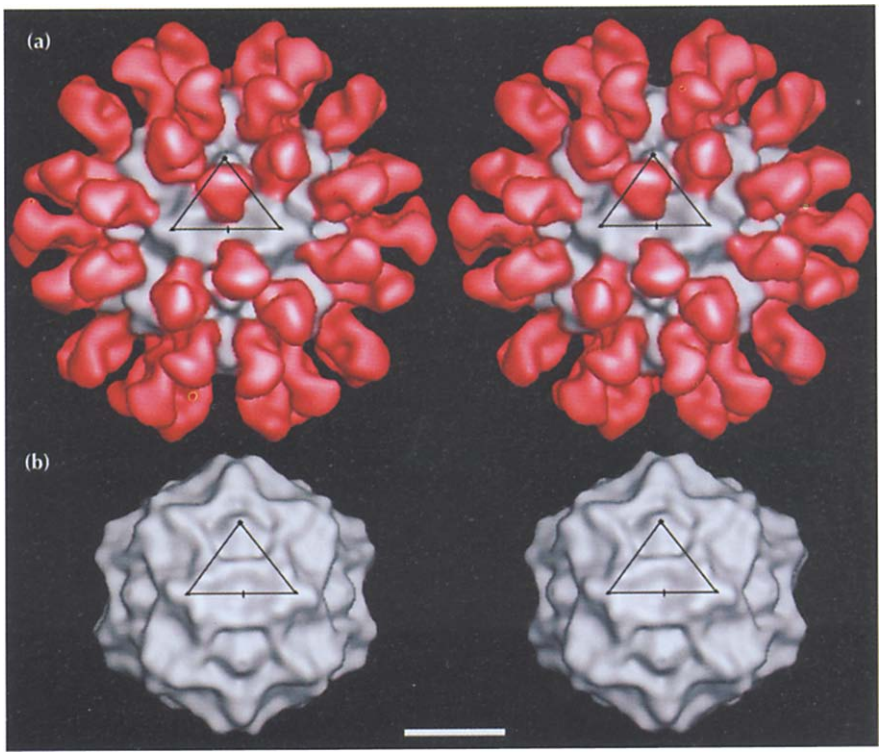

Fig. 3. Stereoviews of the image reconstruction of the CPV:Fab A3B10 complex **(a)** and of the CPV capsid atomic structure **(b)**, both represented at 23 Å resolution. One CPV asymmetric unit, or 1/60 of the $T=1$ virus, is outlined. The five-fold axis is indicated with a filled pentagon, the three-fold axes are indicated by filled triangles and the two-fold axis is indicated by a filled ellipse. The Fab region is colored red and the capsid region is gray. The scale bar indicates 100 Å.

Ala300 to glycine was found to have no effect [15]. Of the residues in the antibody footprint, Thr301 protrudes the farthest from the virus center, although the single mutation, Thr301 to isoleucine, does not inhibit A3B10 binding. In all but one of these escape mutants, there is an addition of one or two negative charges under the antibody footprint. While loop 3 was identified by the escape mutations, no such mutations have been found on loops 1 or 2, which participate in the remainder of the footprint on symmetry-related VP2 subunits. This is consistent with the study of lysozyme–Fab complexes, where mutations have identified only a select subset of interface residues [18,19]. It is also consistent with studies of Reynolds *et al.* [21] who showed that restrictions of the viability of polioviruses containing mutations within an antigenic site limit the range of escape mutations which can be observed by normal selection procedures.

The sequences of the mouse A3B10 heavy (V_H-D_H-L_H) and light (V_κ-J_κ) chain genes were determined (Genbank accession numbers U07813 and U07814, respectively), and the translated amino acid sequence could be readily aligned with the heavy and light chain variable region sequences of mouse Mab HyHEL-5 [22] (Fig. 7). Assuming that the CDR conformations of HyHEL-5 and A3B10 have some similarity, the alignment shows the equivalent A3B10 residues in contact with the CPV surface (Table 3, Fig. 8). Loops 1 and 2 of the heavy chain make by far the most extensive contacts. These also interact with the three residues on CPV which can mutate to escape the neutralization properties of Mab A3B10. CDRs L1 and H3 are considerably longer in A3B10 than in HyHEL-5 and, therefore, might extend the surface contact region. These insertions in A3B10 contain a total of one positively-charged and two negatively-charged residues.

Table 3. Interaction between the HyHEL-5 Fab model and the CPV surface.

CDR	HyHEL-5[a]Fab	A3B10[b]	CPV[c,d]
L1	N30	S35	T391
L2	–		
L3	R92	Y97	T390,T391
H1	T28,S30,D31, Y32,W33	S28,T30,D31 Y32,I33	N85,M87,N231,I232,Y233,**G299 A300**,T301,F303
H2	L52	N52	Q296,S297,T301,**N302**
H3	N100,Y101	G100,Y101	
CPV escape mutations			G299E,A300V,A300D,N302D

[a]At least one non-hydrogen atom within these residues is within 5.0 Å of an atom on the CPV surface. [b]Equivalent residues in A3B10 based on the alignment shown in Fig. 7. [c]At least one non-hydrogen atom within these residues is within 5.0 Å of an atom on the stated CDR loop of the fitted HyHEL-5 structure. [d]Bold residues can carry escape mutations.

The footprint of Fab 17-1A on HRV14 contains a relatively large proportion of charged residues, whereas the footprint of Fab A3B10 on CPV has only one charged residue. The two residues in HRV14 which form escape mutations to Mab 17-1A are negatively charged and form salt bridges between antigen and antibody [10,23,24]. In contrast, none of the three residues in

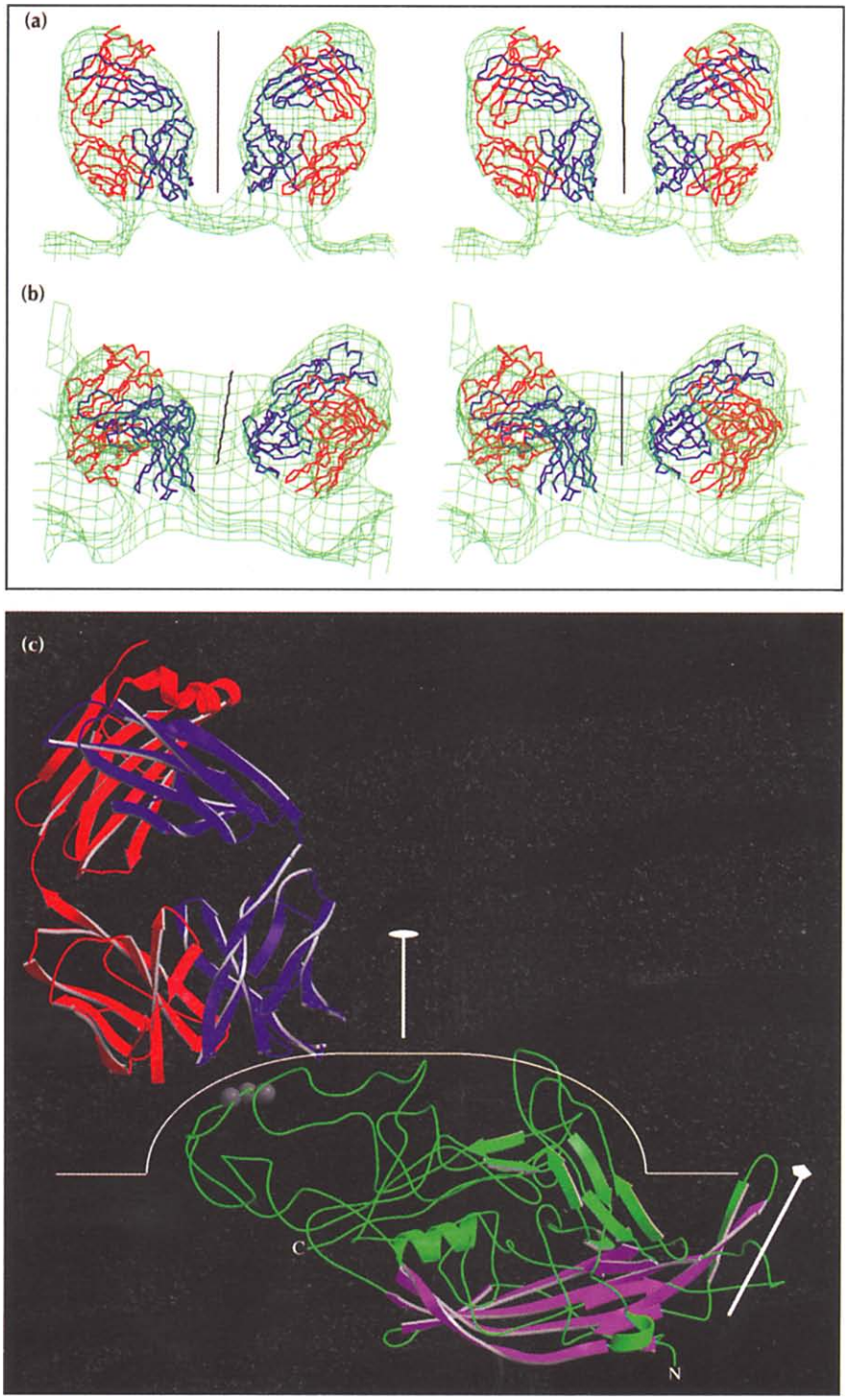

Fig. 4. Results of docking the HyHEL-5 Fab molecule into the electron density of the CPV:Fab A3B10 complex. **(a)** Section through the capsid containing approximately a two-fold axis (indicated with a black line) and a five-fold axis (not shown). The electron density is green, the Fab heavy chain is blue and the light chain is red. (The figure was produced by the programs O [44] and Macinplot [47].) **(b)** As (a) but viewed from a different angle. **(c)** Ribbon diagram, on a larger scale than (a) and (b), showing the interaction between the Fab and one CPV subunit. The orientation is identical to (a). Assuming the preferred Fab orientation, the heavy chain is blue and the light chain is red. The β-barrel domain of CPV is purple while the remainder of the structure is green. The site of escape mutations at residues 299, 300 and 302 are indicated as gray spheres. Two-fold and five-fold axes are indicated. The approximate virus surface is indicated with a white line. (The figure was produced by the programs MOLSCRIPT [48] and Raster3D [49]).

CPV which were found to form escape mutations were charged, although the escape mutations were charged in three of the four cases. As in epitope B of CPV, the escape mutations on HRV14 were centrally located within the footprint of Fab 17-1A on the viral surface. Mutational studies of the peripheral residues in the footprint showed a significant, but lesser, effect on the neutralizing properties of Mab 17-1A on HRV14 [10]. This type of study has not been done on CPV.

Peptide binding

The peptides corresponding to loop 3 exhibited little or no binding to Mab A3B10. In agreement with this is the observation that Mab A3B10 is non-reactive on Western blots from gels of denatured CPV [15]. This suggests that the epitope requires more than the linear sequence of loop 3, and presumably includes neighboring residues on the surface of the virus. Epitope B, identified by escape mutations and now also by elec-

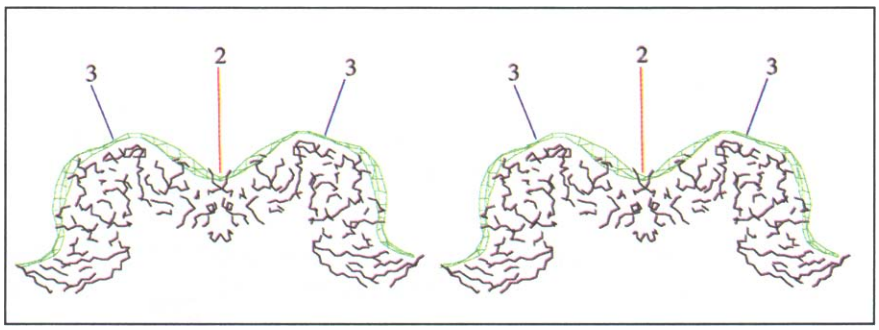

Fig. 5. Central section through CPV showing the external fit of EM density to the known atomic structure of the C_α backbone. Symmetry axes are indicated by numbered lines. The orientation is perpendicular to that of Figs 4a and 4c.

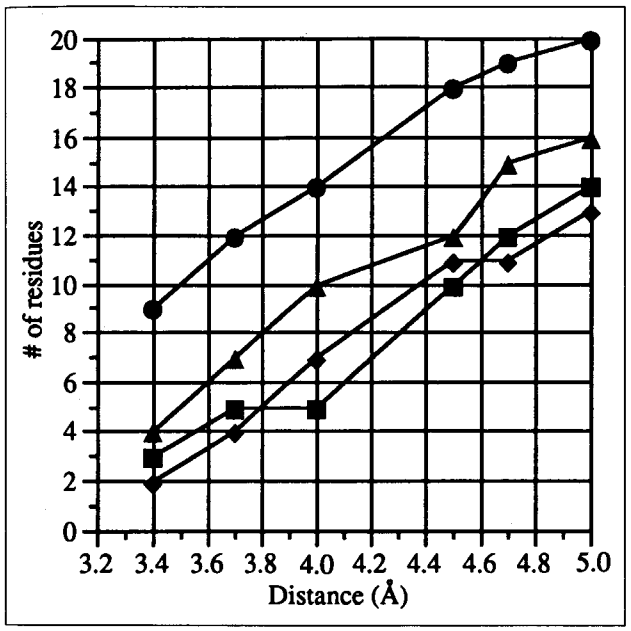

Fig. 6. Comparison of the number of antigen residues in contact between the fitted HyHEL-5 model and CPV (squares) with that of Fab HyHEL-5 complexed with lysozyme (circles). HyHEL-5 is translated radially by 1.00 Å (triangles) and 1.56 Å (diamonds) away from the lysozyme surface. In the latter case, the number of contacts is similar to that found in the CPV:Fab complex.

tron microscopy, does not correspond exactly to the epitope identified by pepscan [14].

Mode of monoclonal antibody binding

The structure of HRV14 complexed with the neutralizing antibody fragment Fab 17-1A [10] showed that the constant domain dimers of the Fabs were almost touching across icosahedral two-fold axes, suggesting that the whole antibody binds bivalently. This was later confirmed by the structure determination of the whole immunoglobulin G (IgG) antibody molecule bound to HRV14 [11]. However, the A3B10 Fab fragment bound to CPV points away from the two-fold axes of the complex (Fig. 4a), suggesting that the IgG binds monovalently. When one of the Fab ends from the known Kol IgG structure [25] was fitted into the densities of one of the A3B10 Fabs, the other Fab end of Kol pointed in a radial direction away from the virus. Thus, the hinge angles of the intact Kol molecule suggest that it would not be possible to bind the A3B10 bivalently to the virus. Even if the constant domains were moved out of the density by adjusting the elbow angle, keeping the variable domains in the density, a whole IgG molecule could not be fitted, because elbow movement would not bring the constant domains closer to the two-fold axes. The monovalent binding of Mab A3B10 is confirmed by the observation that CPV is precipitated by this antibody. Monovalent binding allows virions to cross-link and tends to precipitate virus from solution, whereas bivalent binding does not cause precipitation.

Mechanisms of neutralization

A variety of mechanisms by which viruses become neutralized can be postulated. Firstly, the cross-linking of virions should lower the effective titer of virus in solution, and thus lower the infectivity. A comparison of the ability of IgG and Fab molecules to neutralize CPV would determine the degree to which covalent cross-linking contributes to CPV neutralization. If CPV neutralization is simply a matter of inter-virion cross-linking, the Fabs should not be neutralizing. However, the finding that IgG and Fab neutralized the virus roughly equally well (Fig. 9) in tissue culture, suggests that cross-linking is not the primary cause of neutralization.

Secondly, attachment of viruses to cells might be blocked by covering a receptor binding site with Fab molecules. This would probably require saturation of the virus with Fab or Mab. In CPV, there are multiple neutralizing antigenic sites, and thus a large fraction of the virus surface is covered with neutralizing epitopes. It is unlikely that all of these sites could be involved in a receptor blocking mechanism. Both epitopes A and B, identified by escape mutants, also contain residues which, when mutated, alter cell tropism ([26] and CR Parrish, unpublished data). If the latter is a function of receptor attachment, then the receptor attachment site might be close to, or between, these epitopes. If blocking the receptor is the primary neutralization mechanism, then this is consistent with the ability of Fabs to neutralize with an efficiency close to that of whole IgG.

Thirdly, although receptor attachment might not be blocked, the antibody may sterically hinder the binding of a sufficient number of receptors to the virus,

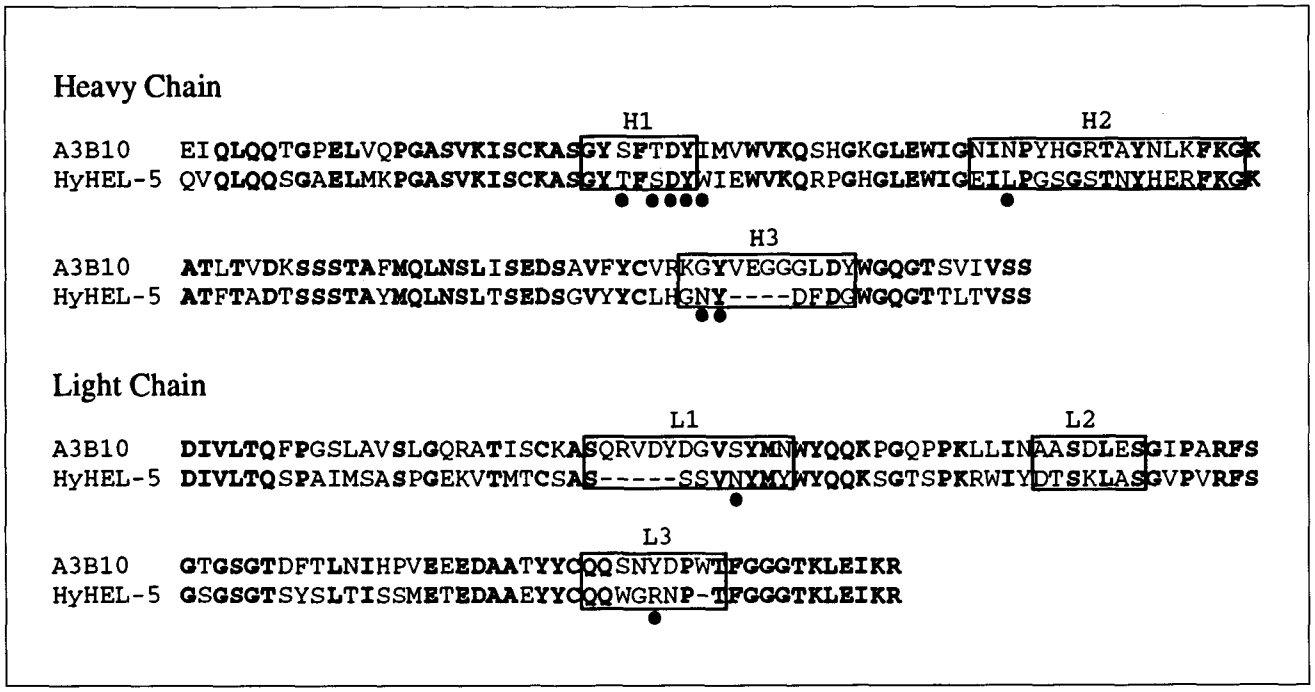

Fig. 7. Alignment of Fab A3B10 and HyHEL-5 heavy and light chain variable domains. Identical regions are indicated in bold faced type. The H1, H2, H3 and L1, L2, L3 CDR loop regions of the heavy and light chains, respectively, are boxed. Those residues of HyHEL-5 which, when fitted into the A3B10 density, are in contact with the CPV surface are marked (●).

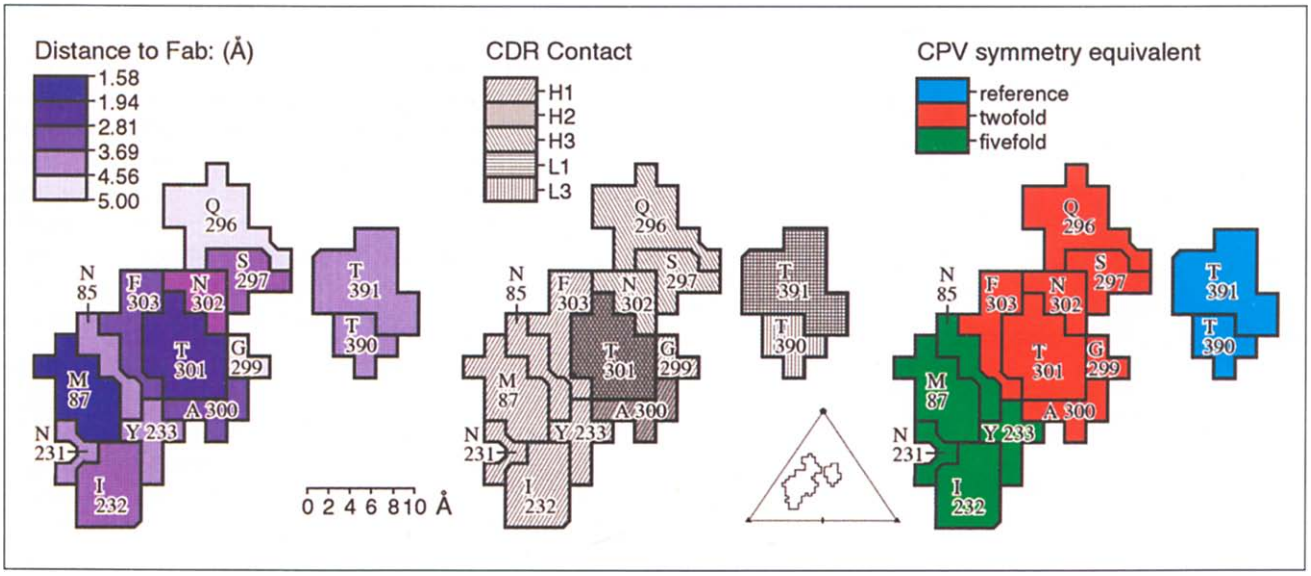

Fig. 8. Enlarged portion of the footprint region on the CPV surface showing the distance of the closest approach between CPV residues and the fitted HyHEL-5 model (left). The distance is indicated by shading, up to a maximum of 5 Å. The location of these residues on the CPV surface is outlined on the icosahedral asymmetric unit (middle inset). The shading of any one amino acid corresponds to the closest approach any non-hydrogen atom within the residue makes to the CPV surface. The separate footprints of each Fab CDR (H1, H2, H3, L1 and L3) are also shown (middle). CPV residues in contact with more than one CDR loop contain the combination of hatching or shading from each of the contacting CDR loops. The conjunction of three symmetry-related subunits (see heavy black lines in Fig. 1) within the footprint is shown on the right. (The figure was produced in part by the program 'Roadmap' [46]).

thereby inhibiting cell entry. In this case, there would be no need for saturating the virus with Fab or Mab to cause neutralization. That may be the case in poliovirus where only a few Mabs of a certain type are needed for neutralization [27].

Finally, if the capsid is stabilized by Fab or Mab binding, neutralization may result from the inhibition of uncoating. A mechanism of capsid stabilizaton by whole antibody binding has been proposed for HRV14 [10]. The CPV:Fab complex suggests a different mode of

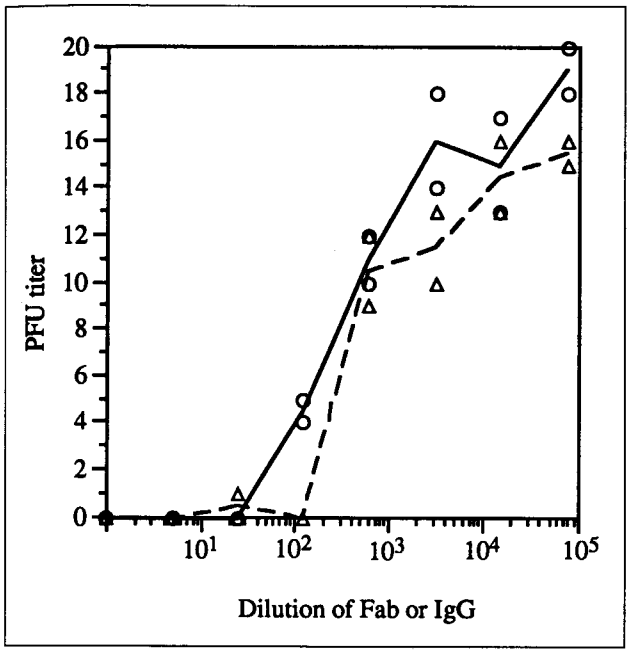

Fig. 9. Plaque neutralization by A3B10 IgG and Fab. Titers of each sample are shown with a triangle for IgG and a circle for Fab. The dashed and solid lines join the mean titers at different dilutions for IgG and Fab, respectively.

capsid stabilization. The footprint of Fab A3B10 is spread over three adjacent two-fold and five-fold-related, non-covalently bound VP2 subunits (Fig. 8, and Fig. 5 in [28]). Thus, Fab binding alone may be able to stabilize the capsid.

The last three mechanisms are consistent with the available data for A3B10, but the first is unlikely.

Biological implications

Viruses are generally prevented from re-infecting individuals that have already mounted an immune response to the virus. A major mechanism for this protection is the development of neutralizing antibodies; when a virus is introduced into an immune individual, neutralizing antibodies block the initial infection of target cells. Perhaps surprisingly for such an important process, the molecular details of the mechanism of antibody neutralization are not well understood. Several possibilities have been proposed, including virus cross-linking to lower the effective titer of virus, competition between antibody and receptor for binding to the the virus, and inhibition of uncoating. In a previous structure of a complex of a virus with neutralizing antibody, an antibody to rhinovirus 14 was found to bind bivalently to two, symmetry-related sites on the virus, excluding virus cross-linking as a mechanism for neutralization. In the structure reported here of canine parvovirus complexed with the Fab fragment of a neutralizing antibody, in contrast, the inclination of the Fab molecule away from the two-fold axis indicates that each antibody can bind to only a single site on a virus particle. The antibody can thus cross-link virus particles, and can indeed precipitate them; however, it is shown here that, at least *in vitro*, the Fab fragment of this antibody can also neutralize virus and so cross-linking cannot be essential for neutralization.

The structure of the virus:Fab complex permits a careful determination of the epitope for antibody binding. There is no evidence that conformational changes occur on binding as seen at 23 Å resolution. The footprint of the antibody covers loop 3 of the CPV coat protein VP2, which is the site of all the known escape mutations for this antibody, and also loops 1 and 2. The escape mutants are centrally located within the footprint. The CPV residues which are in contact with the Fab molecule include residues from symmetry-related protein subunits. Thus, antibody binding may inhibit the uncoating process. The location of the receptor-binding site for CPV has been proposed tentatively on the basis of selected mutations that participate in limiting host range. The proximity of the putative receptor-attachment site and the A3B10-binding site might cause steric hindrance between antibody and receptor. However, as there are 60 such pairs of sites on the virus surface and as the virus is unlikely to be saturated with neutralizing antibody *in vivo*, the effect of steric hindrance is uncertain.

The results reported here limit possible mechanisms by which the virus is neutralized by the A3B10 antibody, and possibly also other antibodies, to inhibition of cell attachment, cell entry and uncoating. Knowledge of the A3B10 binding mode to the virus will now permit further probes of the neutralization mechanism using site-directed mutagenesis of residues in the footprint of the antibody on the viral surface.

Materials and methods

Virus and monoclonal antibody production

Canine parvovirus (CPV) strain CPV-d was propagated in tissue culture and purified as described previously [29]. Final dialysis was against 10 mM Tris-HCl (pH 7.5). The virus concentration was determined spectroscopically.

Negatively-stained virus was examined in the electron microscope to screen samples which had minimal particle aggregation.

Mouse monoclonal antibody (Mab) A3B10, which neutralizes CPV2 [15], was prepared as previously described [29–31]. This antibody, Mab A3B10 is the same as Mab 8 described in [15,30]. Large quantities of Mab were produced both in mouse ascites and in the Cellmax Quad 4 hollow fiber cell culture system (Cellco Corp, Germantown, MD). Hybridomas were grown using high-glucose Dulbecco's modified Eagle medium (GIBCO/Bethesda Research Laboratories, Grand Island, NY), supplemented with 10–15% fetal bovine serum. Antibody was purified by centrifuging the ascites or media for 45 mins at 12 000 rpm in a Sorvall SS-34 rotor. The supernatant was filtered through a 0.22 μ syringe filter, and applied to a 1.2 × 16 cm protein G column at 4°C. The column was washed with 0.1 M phosphate buffer (pH 7.5), and eluted with 0.1 M glycine, pH 3.0. The eluate was dialyzed at 4°C in 0.1 M phosphate buffer, pH 7.5.

Fab generation and purification

Fab fragments were produced by enzymatic digestion with papain [32]. Optimal digestion conditions were first determined using time courses, varying the ratio of enzyme to Mab and the concentration of other reagents. The final conditions contained a papain to Mab ratio of 1:5000. The papain and β-mercaptoethanol mixture was incubated at 37°C for 10 mins, at which time Mab A3B10 was added. The digestion mixture, containing 1.4 mg ml^{-1} Mab A3B10, 3.45 μg ml^{-1} papain, 25 mM β-mercaptoethanol and 1 mM EDTA, was incubated at 37°C for 75 mins. Iodoacetamide was added to a concentration of 10 mM to stop the reaction. The digestion mixture was concentrated and dialyzed against 0.1 M phosphate buffer (pH 7.0) using a Pro-dicon vacuum filtration system (Spectrum) with a 10 000 dalton cutoff to a final volume of approximately 2 ml.

This material was centrifuged at 12 500 *g* and the supernatant applied to a Mono Q® column (FPLC® from Pharmacia) in batches of 8–10 mg at a flow rate of 1 ml min^{-1} and washed with solvent A (20 mM phosphate, pH 8.6). The Fab was eluted with a gradient of 0–7.5 % solvent B (solvent A + 1 M NaCl). The sample was analyzed by isoelectric focusing (IEF), using a PhastSystem™ (Pharmacia). Fractions consisting primarily of the pI 7.2 Fab band were pooled and dialyzed against 50 mM 4-morpholineethanesulfonic acid (MES) (pH 6.1), then concentrated using a Centricon-10 (Amicon) ultra-filter. This sample was centrifuged, and the supernatant was applied to a Mono S® column, which was run isocratically with the same MES buffer. Fractions from multiple runs were analyzed by IEF and pooled. They were dialyzed against 20 mM Tris-HCl (pH 7.5) buffer using a Centricon-10 ultra-filter.

Complex formation and purification

Various Fab:CPV ratios were sampled to determine the optimum conditions for microscopy. All samples were first examined by negative-stain electron microscopy (EM) to establish that the virus was saturated with Fab and exhibited minimal aggregation. Having established suitable conditions, unbound Fab was removed by repeated washing of the complex through a centrifuge microconcentrator (Spectrum) with a molecular weight cutoff of 300 000 daltons. The filtrate was collected and centrifuged at 12 500 *g* to remove large aggregates. Samples were examined by negative-stain EM, and the best were used for cryo-EM.

Peptide binding

Two nonameric peptides (QSEGATNFG and ATNFGDIGV) and one heptameric peptide (QSEGATN), corresponding to the CPV surface epitope identified from the EM and escape mutant results, were synthesized using fluorenyl methoxy carbonyl (Fmoc) methods (Applied Biosystems). Binding of these peptides to the Mab was assayed by enzyme-linked immunosorbent assay (ELISA), where peptides were applied directly to the polystyrene plate followed by Mab A3B10 incubation. No significant binding of Mab to peptide was observed. In addition, neither of these peptides was able to compete with CPV for binding to A3B10 as tested with an ELISA.

Neutralization

The virus neutralization efficiencies of IgG and Fab were compared using a plaque reduction assay [15]. Two five-fold dilution series were prepared for both A3B10 IgG (starting at 10 μg ml^{-1}) and Fab (also starting at 10 μg ml^{-1} and, therefore, corresponding to a molar ratio of one to three, respectively). A 150 μl aliquot of each dilution was mixed with 150 μl of CPV [containing 16–20 plaque forming units (PFU)], incubated for 1 h at 37°C; the number of surviving PFUs was then determined (Fig. 9).

Cloning and sequencing of the variable regions of the A3B10 immunoglobulin genes

The total RNA was isolated from the hybridoma after lysis in a buffer containing 4 M guanidinium thiocyanate, and pelleted through 5.7 M CsCl at 175 000 *g* for 18 h. The first strand cDNA synthesis from the RNA was performed with avian leukosis virus reverse transcriptase, using oligo(dT) as a primer [33]. The RNA was mixed with combinations of heavy and light chain primers (Ig-Prime kit obtained from Novagen, Madison, WI). The DNA products were amplified by polymerase chain reaction, generally as described by Jones and Bendig [34] and Coloma and Larrick [35]. The products obtained were cloned into a vector containing a single T-residue overhang (T-Vector, Novagen, Madison, WI) and the heavy and light chain V-region clones obtained were sequenced in both orientations using SP6 and T7 primers with modified T7 DNA polymerase (Sequenase, United States Biochemical Corp., Cleveland, OH) and ^{35}S-dATP label.

Microscopy and image reconstruction

Images of the frozen-hydrated samples of the CPV:Fab complex were recorded using established procedures [36,37]. Aliquots of aqueous samples (~3 μl at ~2 mg ml^{-1}) were applied to holey, carbon-coated EM grids. Excess sample was blotted with filter paper and the grids were then immediately plunged into liquid ethane. The vitrified samples were transferred into liquid nitrogen and maintained at a temperature of approximately −168°C in a Gatan Model 626 cryo-transfer holder (Gatan Inc., Warrendale, PA). Micrographs were recorded under minimal dose conditions (< 20 e$^-$ Å^{-2}), at ~49 000 × magnification with the objective lens underfocused ~0.8 μm in a Philips EM420 electron microscope (Philips Electronics Instruments, Mahwah, NJ).

Selection and digitization (at 25 μm intervals, corresponding to 5.1 Å spacings in the specimen) of micrographs was carried out essentially as described [37]. Two independent three-dimensional reconstructions were computed, both starting from an identical data set consisting of 117 digitized particle images. We computed both reconstructions to a final resolution of 23 Å using 40 particle images in each instance. The images were screened using a model-based approach that helped determine the relative orientations of all 117 particles and provided quantitative criteria to select the 'best' (self-consistent) data ([38] and TS Baker and RH Cheng, unpublished data).

The first model was a low resolution (46 Å), single-particle reconstruction that was obtained using common-lines and Fourier-Bessel procedures [39]. This model provided a reference for cross-correlation procedures from which the orientations of all other particles could be obtained with an initial accuracy of at least 1° in angular increment. Once an intermediate three-dimensional reconstruction was achieved, this then served as an improved model for a subsequent cycle of orientation and translation (phase origin) refinement, also employing cross-common lines procedures [40,41]. This scheme was carried out for a total

of three cycles, yielding a final 40-particle reconstruction to 23 Å resolution.

A second CPV:Fab model was synthesized by taking the atomic structure of the native CPV [6] and docking to it 60 copies of the atomic structure of the Fab fragment Kol [25]. The Kol structure was positioned with the Fab pseudo-dyad in a near-radial orientation and with the variable dimer abutted against the site of the A3B10 epitope [15]. Because the precise location of the Fab footprint on the viral surface was unknown, the rotational orientation about the pseudo-dyad was a random choice. This 'atomic' CPV:Fab model (non-hydrogen atoms only) was then used to produce a set of structure factors from which a 25 Å resolution density map was computed and used in the same manner as the single-particle reconstruction, but only for densities between radii of 85–130 Å, to measure and refine the translational and orientational parameters of the 117 particles in the data set. The final 40-particle reconstruction included 26 (65 %) of the same images used to compute the first reconstruction. The Fab molecules in the two separate reconstructions were identically oriented with respect to the icosahedral axes of the virus, but this orientation differed by ~60° from that in the initial atomic model used in the second procedure described above. Quantitative comparison of the two independent reconstructions showed excellent agreement (correlation coefficients nearly equal to 1.0 for densities within radial limits of 100 Å and 200 Å), thus indicating the high reliability and reproducibility of the reconstructed density features in the CPV:Fab complex. The second reconstruction, after appropriate corrections were applied to it to compensate for the effects of the microscope contrast transfer function [38], was used to carry out the HyHEL-5 docking studies reported here.

The micrographs are a projection of the randomly oriented three-dimensional virion onto a two-dimensional surface and, hence, direct information about the hand of the reconstruction is lost. However, as the structure of CPV is known, the correct choice of the two possible hands of the reconstruction can be determined by visual comparison of the complex structure with that of the known CPV structure. There are sufficient surface features for the apparent hand to be readily apparent. The hand was also determined by comparison of the *R*-factor $[R = \Sigma|(\rho_{cryo} - \kappa\rho_{xray})|/\Sigma\rho_{cryo}]$ between the electron densities for the EM complex with that of the X-ray structure in a shell corresponding to the capsid region.

Docking the atomic Fab model in the map

The radial scale of an image reconstruction from cryo-EM data is not accurate, due to lack of precise knowledge of the image magnification in the absence of internal calibration standards [42,43]. Therefore, the CPV atomic coordinates were used to determine the interpixel spacing (grid spacing) of the EM map. Only the density within a spherical shell of inner radius 100 Å and outer radius 140 Å, corresponding approximately to the protein volume of a CPV capsid, was used in scale determination. The grid intervals of the EM map were considered systematically from 4.5 Å to 5.5 Å in steps of 0.04 Å for comparison with the atomic model. If the original EM scale had been perfect, the grid interval would be 5.1 Å. R-factors and correlation coefficients were calculated to obtain the best agreement between the CPV and the EM density to determine the optimum scale. It was found that the EM map should have had an interval of 4.96 Å, corresponding to a shrinkage of about 3.8 Å of the viral radius.

Fab atomic models in the Brookhaven data base were visually compared for their fit to the Fab region of the EM map. The major difference that affected the visual quality of the fit was the elbow angle between the variable and constant dimer. The best fit appeared to be for HyHEL-5, whose structure had been determined to 2.6 Å resolution [18]. The elbow angle for HyHEL-5 is approximately 155°, providing some asymmetry to guide the unique fitting of the model to the density.

HyHEL-5 was manually positioned into the electron density map using the program O [44]. The flattened Fab electron density and depression around the elbow angle left only two possible trial docking arrangements. Matrices encompassing the rotation and translation between the original coordinates and the final docked coordinates were determined using O and used subsequently as the initial positions in refinement. The Fab position and orientation were subsequently refined by a least-squares reciprocal space method. The EM electron density was first normalized by adding a constant to each density value to assure that the sum of the density within the unit cell was zero. To minimize effects of solvent, nucleic acid and noise, an atomic mask was generated for the virion from the CPV atomic coordinates. The Fab envelope could then be identified as the density that was significantly above the background and included in the mask. All regions of the map which were not within the mask were considered part of the nucleic acid or solvent. This part of the map was back-transformed and vectorially added to the structure factors derived from the atomic structure of the CPV:Fab complex.

The Fab position was then refined, using reciprocal space rigid-body refinement in the program X-PLOR (version 3.1) [45], to minimize the difference between phase and amplitude information. A linear scale factor between these two sets of structure amplitudes was obtained by finding the best fit for the calculated structure amplitudes to those obtained by back-transforming the whole of the normalized EM map. The refinement minimized

$$S = \sum_{hkl} \left[(A_{obs} - kA_{calc})^2 + (B_{obs} - kB_{calc})^2 \right]^2$$

where A_{obs} and B_{obs} are the real and imaginary components of the structure factor F_{obs} representing the CPV:Fab complex electron density derived from the EM structure. A_{calc} and B_{calc} are the real and imaginary components of the structure factors F_{calc} obtained from the atomic positions in the CPV particle and the 60 Fab molecules, where;

$$F_{obs} = \int_{V} \rho_{EM}(\mathbf{x}) e^{2\pi i h \cdot \mathbf{x}} d\mathbf{x} - \int_{V_{inv}} \rho_{EM}(\mathbf{x}) e^{2\pi i h \cdot \mathbf{x}} d\mathbf{x},$$

ρ_{EM} is the cryo-EM image reconstructed density, V is the volume of the unit cell and V_{inv} is the volume of the unit cell which does not include the virus nor the Fab structure. Also, k is a scale factor between observed and calculated structure amplitudes. The scale factor, k, and overall temperature factor were determined initially, followed by the refinement of the three angles and three translations that define the orientation and position of the Fab fragment. Chemical interactions were not considered in the refinement because the atomic structure of the Fab A3B10 molecule was not known with precision. The convergence was monitored by observing the conventional 'scalar' *R*-factor between F_{obs} and F_{calc} as well as the 'vector' *R*-factor defined as:

$$\frac{\sum_{hkl} \left[(A_{obs} - kA_{calc}) + (B_{obs} - kB_{calc}) \right]^2}{\sum_{hkl} |F_{obs}|}$$

The inclusion of the structure factors representing the solvent and nucleic acid regions, rather than a simple flattening or averaging, should enhance the agreement between observed and calculated structure factors as the calculated structure factors will then more accurately represent the observed electron density

map. For the A3B10:CPV complex, the final *R*-factor was 35% for one orientation and 38° for the other approximately 180°-related fit with respect to data between 500 Å and 25 Å resolution. These two fits correspond to an interchange of the heavy and light chain positions. The better fit was used in determining the footprint, although the amino acids identified as being in the footprint would not be substantially changed in using the alternative orientation.

Footprint and buried surface area determination

After rigid-body refinement of the Fab position, the final Fab coordinates were used to determine which residues of CPV were in contact. The contact residues were determined by calculating all of the interatomic distances between CPV and the Fab and selecting the atomic contacts within distance cutoffs of 3.4 Å, 3.7 Å, 4.0 Å, 4.5 Å, 4.7 Å and 5.0 Å. The surface area of the contact region between CPV and Fab was determined using the Lee and Richards algorithm [17] with a 1.7 Å probe radius, as implemented in the program X-PLOR (version 3.1) [45].

Acknowledgments: We are grateful to Thomas Smith, Elaine Chase and Mavis Agbandje for their instruction and help in growing monoclonal antibodies in a cell culture system. The work was supported by a National Institutes of Health and a National Science Foundation grant to MGR, a National Institutes of Health and a National Science Foundation grant to TSB, a National Institutes of Health grant to CRP and MGR and a Lucille P Markey Foundation Award to expand structural studies at Purdue University to MGR.

References

1. Parrish, C.R. (1990). Emergence, natural history, and variation of canine, mink, and feline parvoviruses. *Adv. Virus Res.* **38**, 403–450.
2. Studdert, M.J. (1990). Tissue tropism of parvoviruses. In *CRC Handbook of Parvoviruses.* (Tijssen, P., ed), Vol II, pp. 3–27, CRC Press, Inc., Boca Raton, FL.
3. Anderson, M.J., *et al.*, & Pereira, M.S. (1983). Human parvovirus, the cause of erythema infectiosum (fifth disease)? *Lancet* **i**, 1378.
4. Anderson, M.J., Lewis, E., Kidd, J.M., Hall, S.M. & Cohen, B.J. (1984). An outbreak of erythema infectiosum associated with human parvovirus infection. *J. Hyg.* **93**, 85–93.
5. Siegl, G. (1984). Biology and pathogenicity of autonomous parvoviruses. In *The Parvoviruses.* (Berns, K.I., ed), pp. 297–362, Plenum Press, New York & London.
6. Tsao, J., *et al.*, & Parrish, C.R. (1991). The three-dimensional structure of canine parvoviruses and its functional implications. *Science* **251**, 1456–1464.
7. Tattersall, P. & Gardiner, E.M. (1990). Autonomous parvovirus-host–cell interactions. In *CRC Handbook of Parvoviruses.* (Tijssen, P., ed), Vol I, pp. 111–121, CRC Press, Inc., Boca Raton, FL.
8. Tattersall, P. & Cotmore, S.F. (1990). Reproduction of autonomous parvovirus DNA. In *CRC Handbook of Parvoviruses.* (Tijssen, P., ed), Vol I, pp. 123–140, CRC Press, Inc., Boca Raton, FL.
9. Agbandje, M., McKenna, R., Rossmann, M.G., Strassheim, M.L. & Parrish, C.R. (1993). Structure determination of feline panleukopenia virus empty particles. *Proteins* **16**, 155–171.
10. Smith, T.J., *et al.*, & Baker, T.S. (1993). Structure of human rhinovirus complexed with Fab fragments from a neutralizing antibody. *J. Virol.* **67**, 1148–1158.
11. Smith, T.J., Olson, N.H., Cheng, R.H., Chase, E.S. & Baker, T.S. (1993). Structure of a human rhinovirus-bivalently bound antibody complex: implications for viral neutralization and antibody flexibility. *Proc. Natl. Acad. Sci. USA* **90**, 7015–7018.
12. Rimmelzwaan, G.F., Carlson, J., UytdeHaag, F.G.C.M. & Osterhaus, A.D.M.E. (1990). A synthetic peptide derived from the amino acid sequence of canine parvovirus structural proteins which defines a B cell epitope and elicits antiviral antibody in BALB-c mice. *J. Gen. Virol.* **71**, 2741–2745.
13. López de Turiso, J.A., *et al.*, & Casal, J.I. (1991). Fine mapping of canine parvovirus B cell epitopes. *J. Gen. Virol.* **72**, 2445–2456.
14. Langeveld, J.P.M., *et al.*, & Meloen, R.H. (1993). B-cell epitopes of canine parvovirus: distribution on the primary structure and exposure on the viral surface. *J. Virol.* **67**, 765–772.
15. Strassheim, M.L., Gruenberg, A., Veijalainen, P., Sgro, J.Y. & Parrish, C.R. (1994). Two dominant neutralizing antigenic determinants of canine parvovirus are found on the threefold spike of the virus capsid. *Virology* **198**, 175–184.
16. Wang, G., Porta, C., Chen, Z., Baker, T.S. & Johnson, J.E. (1992). Identification of a Fab interaction footprint site on an icosahedral virus by cryoelectron microscopy and X-ray crystallography. *Nature* **355**, 275–278.
17. Lee, B. & Richards, F.M. (1971). The interpretation of protein structures: estimation of static accessibility. *J. Mol. Biol.* **55**, 379–400.
18. Sheriff, S., *et al.*, & Davies, D.R. (1987). Three-dimensional structure of an antibody–antigen complex. *Proc. Natl. Acad. Sci. USA* **84**, 8075–8079.
19. Davies, D.R., Sheriff, S. & Padlan, E.A. (1988). Antibody–antigen complexes. *J. Biol. Chem.* **263**, 10541–10544.
20. Wilson, I.A. & Stanfield, R.L. (1993). Antibody–antigen interactions. *Curr. Opin. Struct. Biol.* **3**, 113–118.
21. Reynolds, C., Page, G., Zhou, H. & Chow, M. (1991). Identification of residues in VP2 that contribute to poliovirus neutralization antigenic site 3B. *Virology* **184**, 391–396.
22. Hartman, A.B., Mallett, C.P., Sheriff, S. & Smith-Gill, S.J. (1988). Unusual joining sites in the H and L chains of an anti-lysozyme antibody. *J. Immunol.* **141**, 932–936.
23. Sherry, B. & Rueckert, R. (1985). Evidence for at least two dominant neutralization antigens on human rhinovirus 14. *J. Virol.* **53**, 137–143.
24. Sherry, B., Mosser, A.G., Colonno, R.J. & Rueckert, R.R. (1986). Use of monoclonal antibodies to identify four neutralization immunogens on a common cold picornavirus, human rhinovirus 14. *J. Virol.* **57**, 246–257.
25. Marquart, M., Deisenhofer, J., Huber, R. & Palm, W. (1980). Crystallographic refinement and atomic models of the intact immunoglobulin molecule Kol and its antigen-binding fragment at 3.0 Å and 1.9 Å resolution. *J. Mol. Biol* **141**, 369–391.
26. Chapman, M.S. & Rossmann, M.G. (1993). Structure, sequence, and function correlations among parvoviruses. *Virology* **194**, 491–508.
27. Icenogle, J., Shiwen, H., Duke, G., Gilbert S., Rueckert, R. & Anderegg, J. (1983). Neutralization of poliovirus by a monoclonal antibody: kinetics and stoichiometry. *Virology* **127**, 412–425.
28. Wu, H. & Rossmann, M.G. (1993). The canine parvovirus empty capsid structure. *J. Mol. Biol.* **233**, 231–244.
29. Parrish, C.R., Carmichael, L.E. & Antczak, D.F. (1982). Antigenic relationships between canine parvovirus type-2 feline panleukopenia virus and mink enteritis virus using conventional antisera and monoclonal antibodies. *Arch. Virol.* **72**, 267–278.
30. Parrish, C.R. & Carmichael, L.E. (1983). Antigenic structure and variation of canine parvovirus type-2, feline panleukopenia virus, and mink enteritis virus. *Virology* **129**, 401–414.
31. Parrish C.R., O'Connell, P.H., Evermann, J.F. & Carmichael, L.M. (1985). Natural variation of canine parvovirus. *Science* **230**, 1046–1048.
32. Porter, R.R. (1959). The hydrolysis of rabbit γ-globulin and antibodies with crystalline papain. *Biochem. J.* **73**, 119–126.
33. Sambrook, J., Fritsch, E.F. & Maniatis, T. (1989). *Molecular Cloning, a Laboratory Manual* (2nd edn), Cold Spring Harbor Laboratory Press, Cold Spring Harbor, NY.
34. Jones, S.T. & Bendig, M.M. (1991). Rapid PCR-cloning of full-length mouse immunoglobulin variable regions. *Biotechnology* **9**, 88–89.
35. Coloma, M.J. & Larrick, J.W. (1991). Primer design for the cloning of immunoglobulin heavy-chain leader-variable regions from mouse hybridoma cells using the PCR. *Biotechniques* **11**, 152–156.
36. Adrian, M., Dubochet, J., Lepault, J. & McDowall, A.W. (1984). Cryo-electron microscopy of viruses. *Nature* **308**, 32–36.
37. Baker, T.S., Drak, J. & Bina, M. (1988). Reconstruction of the three-dimensional structure of simian virus 40 and visualization of the chromatin core. *Proc. Natl. Acad Sci. USA* **85**, 422–426.
38. Cheng, R.H., Reddy, V.S., Olson, N.H., Fisher, A.J., Baker, T.S. & Johnson, J.E. (1994). Functional implications of quasi-equivalence

in a $T=3$ icosahedral animal virus established by cryo-electron microscopy and X-ray crystallography. *Structure* **2**, 271–282.
39. Venie-Bryan, C. & Fuller, S.D. (1994). The organization of the spike complex of Semliki Forest virus. *J. Mol. Biol.* **236**, 572–583.
40. Crowther, R.A. (1971). Procedures for three-dimensional reconstruction of spherical viruses by Fourier synthesis from electron micrographs. *Philos. Trans. R. Soc. Lond. [Biol.]* **261**, 221–230.
41. Fuller, S.D. (1987). The T=4 envelope of Sindbis virus is organized by interactions with a complementary T=3 capsid. *Cell* **48**, 923–934.
42. Olson, N.H. & Baker, T.S. (1989). Magnification calibration and the determination of spherical virus diameters using cryo-microscopy. *Ultramicroscopy* **30**, 281–298.
43. Belnap, D.M., Grochulski, W.D., Olson, N.H. & Baker, T.S. (1993). Use of radial density plots to calibrate image magnification for frozen-hydrated specimens. *Ultramicroscopy* **48**, 347–358.
44. Jones, T.A., Zou, J.-Y., Cowan, S.W. & Kjeldgaard, M. (1991). Improved methods for building protein models in electron density maps and the location of errors in these models. *Acta Crystallogr. A* **47**, 110–119.
45. Brünger, A.T., Kuriyan, J. & Karplus, M. (1987). Crystallographic *R* factor refinement by molecular dynamics. *Science* **235**, 458–460.
46. Chapman, M.S. (1993). Mapping the surface properties of macromolecules. *Protein Sci.* **2**, 459–469.
47. Smith, T.J. (1990). *MACINPLOT* - a program to display electron density and atomic models on the Macintosh personal computer. *J. Appl. Crystallogr.* **23**, 141–142.
48. Kraulis, P.J. (1991). MOLSCRIPT: a program to produce both detailed and schematic plots of protein structures. *J. Appl. Crystallogr.* **24**, 946–950.
49. Bacon, D.J. & Anderson, W.F. (1988). A fast algorithm for rendering space-filling molecule pictures. *J. Mol. Graphics* **6**, 219–220.

Received: **5 Apr 1994;** revisions requested: **19 Apr 1994;** revisions received: **3 May 1994.** Accepted: **4 May 1994.**